



Area-Selective Atomic Layer Deposition of Platinum on YSZ Substrates Using Microcontact Printed SAMs

Xirong Jiang^a and Stacey F. Bent^{b,z}

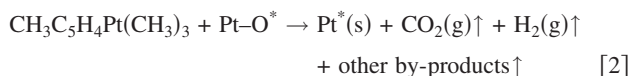
^aDepartment of Physics and ^bDepartment of Chemical Engineering, Stanford University, Stanford, California 94305, USA

Using (methylcyclopentadienyl)trimethylplatinum (MeCpPtMe₃) and oxygen as precursors, Pt has been deposited by atomic layer deposition (ALD) on the surfaces of yttria-stabilized zirconia (YSZ), a solid oxide electrolyte, as well as on oxide-covered silicon. Ex situ analyses have been carried out to examine the properties of both as-deposited and postannealed Pt films. X-ray photoelectron spectroscopy measurements demonstrate that there are no detectable impurities in the as-deposited Pt films, and four-point probe measurements show that the resistivity for a 30.2 nm film is as low as 18.3 μΩ cm. The use of area-selective ALD to deposit patterned Pt has also been investigated. By coating these same substrates with octadecyltrichlorosilane (ODTS) self-assembled monolayers (SAMs), Pt ALD can be successfully blocked. Furthermore, it is shown that by transferring the ODTS SAMs to the substrates by microcontact printing (μCP) using patterned stamps, platinum thin films are grown selectively on the SAM-free surface regions. Features with sizes as small as 2 μm have been deposited by this combined ALD-μCP method; the resolution is limited by the printed pattern and, likely, can be achieved at dimensions significantly smaller than a micrometer. © 2007 The Electrochemical Society. [DOI: 10.1149/1.2789301] All rights reserved.

Manuscript submitted April 18, 2007; revised manuscript received August 15, 2007. Available electronically October 11, 2007.

Pt has enormous application prospects in catalysis and microelectronics.^{1,2} For example, due to its chemical stability in both oxidative and reductive environments, and its excellent electrical properties at high temperatures,³ Pt is used as the electrode material in nonvolatile ferroelectric random access memory devices and high dielectric capacitors. It also exhibits excellent catalytic activity for a number of reactions, including the O₂ reduction reaction at the cathode of a solid oxide fuel cell (SOFC), and is especially useful at the lower operating temperatures (below 600°C) that are desired for integratable fuel cell systems.⁴

We are exploring whether the technique of atomic layer deposition (ALD) can be used to deposit Pt⁵ on an yttria-stabilized zirconia (YSZ) solid oxide electrolyte for the catalyst in SOFCs. ALD is a thin-film deposition method that can achieve excellent thickness control down to the subnanometer scale and may provide the ability to deposit ultrathin Pt films required for complex fuel cell geometries.⁶ In addition, we are working to apply area selective ALD to deposit patterned thin films of Pt for use as the current collector grid of the SOFC. The ALD method relies on sequential saturated surface reactions, which result in the formation of up to one monolayer each cycle. The mechanism of successive self-terminating growth steps in ALD, and the pulse sequence, which eliminates gas-phase reactions, confines the reaction to the substrate surface.^{6,7} For example, the Pt ALD process includes two self-limiting chemical reactions, repeated in the alternating ABAB sequences shown below



where the asterisks represent the surface species.^{5,8,9} Because the ALD process is very sensitive to the surface functional groups, it offers an ideal method for selective deposition of thin films on patterned substrates in which the substrate surface properties are spatially modified.^{10,11}

We have shown in earlier work that microcontact printed (μCP) self-assembled monolayers (SAMs) can be used to achieve spatially patterned deposition of HfO₂ by area selective ALD.¹² Others have used a similar approach for selective ALD of films such as TiO₂, ZnO, and Ru.¹³⁻¹⁸ SAMs are thin organic films that spontaneously form on solid surfaces and are well known for modifying the physical, chemical, and electrical properties of semiconducting, insulat-

ing, and metallic surfaces. Their potential applications include the control of wetting and adhesion, tribology, chemical sensing, ultrafine-scale lithography, and protection of metals against corrosion.¹⁹⁻²¹ In our area-selective ALD process, the SAM is used to modify the chemical properties of the substrate surface such that it resists the atomic layer deposition chemistry.

In this paper, we briefly describe the characterization of the Pt ALD process, demonstrate the properties of the as-deposited and postannealed Pt thin film grown on the substrates of both Si and YSZ, and illustrate an area-selective deposition process to achieve spatially patterned Pt on the same substrates. Our approach to area-selective deposition consisted of two key steps. First, the patterned SAMs were formed using microcontact printing (μCP). Second, the Pt thin films were selectively deposited onto the SAM-patterned Si and YSZ substrates by ALD.

Experimental

All chemical reagents, including octadecyltrichlorosilane (ODTS) (97%), tridecafluoro-1,1,2,2-tetrahydrooctyltrichlorosilane (FOTS) (97%), toluene (anhydrous, 99.8%), and chloroform (99%), used to form SAMs, were purchased from Aldrich (Milwaukee, Wisconsin). Poly(dimethylsiloxane) (PDMS) (Sylgard 184) was purchased from Dow Corning. The (methylcyclopentadienyl)trimethylplatinum (MeCpPtMe₃) (99%) precursor for ALD was obtained from Strem. All these reagents and gases were used directly without further treatment. Nitrogen gas (99.9995%) was obtained from Praxair and purified by a gas filter from Nanochem (model no.: PF-25) before use.

Si substrates were cut from Si(100) wafers purchased from Si-Tech, Inc. (p-type with boron dopant; resistivity of 1.0–10.0 Ω cm). Si substrates were cleaned by a standard piranha process, resulting in a chemical oxide-coated silicon substrate. Thin-film YSZ substrates, deposited by ALD on Si(100), were provided by Friedrich Prinz's group at Stanford University.²² Two steps were used to clean the YSZ substrates.²³ First, the substrates were rinsed ultrasonically, twice, for 5 min in ethyl alcohol in order to remove grease. After the first rinse, the ethyl alcohol was renewed. Following the ethyl alcohol rinses, the YSZ substrates were exposed to rf oxygen plasma for 10 min to make the surface hydrophilic.

The samples were loaded into a custom-built, flow-type ALD system. Pt thin films were deposited onto Si and YSZ substrates using MeCpPtMe₃ and air, providing a source of oxygen, as ALD precursors. The air was dried through a desiccant air dryer to a dew point temperature of -45.5°C before use. Nitrogen was used as both a purging gas and a carrier gas. The MeCpPtMe₃ and air were kept at 50°C and 21°C, respectively. A regular ALD cycle consisted of a

^z E-mail: sbent@stanford.edu

2 s exposure to MeCpPtMe₃, a 12 s N₂ purge, a 2 s exposure to dry air, and a 12 s N₂ purge. The total flow rate of the N₂ was 15 sccm. For the area-selective area ALD processes, the purging time was extended to 30 s to ensure removal of any unreacted precursor from the substrate. Except for the study of substrate temperature dependence, for which the temperature was varied, Pt thin films were grown with the substrate temperature at 285°C at a reactor pressure of 700 mTorr for a varying number of cycles.

All procedures for SAM formation were performed in a dry glove box at room temperature. Previous studies^{10,11} have shown that the deactivating effect of ODTS SAMs depends on its quality and that densely packed SAMs are required for good deactivation. For preparation of a densely packed, continuous (unpatterned) film, the cleaned Si and YSZ substrates were dipped in 10 mM solutions of ODTS in toluene for two days without disturbance. Shorter dipping times were also examined to study the dependence of the resist quality on the ODTS SAM formation time. The unpatterned ODTS-coated samples were examined using water contact angle measurements and ellipsometry before loading them into the ALD reactor.

It was found that the working environment was very important for the SAM formation, as previously reported in the literature.²⁴⁻²⁶ In our initial experiments, we used a simple dry-air-purged glove box. However, with this system, we found there was a high likelihood of forming ODTS multilayers instead of monolayers, due to the water content in the glove box, leading to bulk polymerization of the silane before it reacted with the surface. We subsequently switched to a nitrogen-purged commercial glove box (from Vacuum Atmosphere Co.) that had an oxygen content below 0.1 ppm and a water content below 0.7 ppm. Using this glove box, however, only partial growth or sometimes no growth of ODTS SAMs was obtained. The poor growth of the SAM in the higher-quality glove box was attributed to the lack of water because small amounts of water are necessary in the silylation and cross-linking reactions.^{19,27-29} Thus, for the remaining SAM experiments, we used the simpler glove box, but took greater care in eliminating sources of water.

Patterned monolayers on the Si and YSZ substrates were made using standard μ CP procedures.³⁰ Masters were fabricated from patterned silicon wafers by conventional photolithography. The masters had a mesh structure with lines and spacings of dimensions from 2 μ m to 50 μ m and a line depth of 7 μ m. The PDMS stamps were cast according to a previously reported procedure.³⁰ The prepared PDMS stamps were then wetted with a 10 mM ODTS or 10 mM FOTS solution, both with toluene as the solvent, and dried by nitrogen flow. The dimensions of the ODTS soaked stamp will change with wetting time because the PDMS stamp swells in the toluene solution; consequently, the wetting time was held to 1 min, a time that we have found can retain the patterns on the stamp. Subsequently, the stamp was placed in contact with the Si or YSZ substrate at room temperature for varying lengths of time. After peeling off the stamp, the samples were rinsed with toluene and chloroform, sequentially, and dried by nitrogen flow, leaving behind patterned SAMs formed on the substrates. These substrates were then loaded into the ALD reactor for Pt deposition.

The film thickness of Pt was measured by ellipsometry and X-ray reflectometry (XRR). A single-wavelength ellipsometer was used for the measurement of Pt thin films at thicknesses below \sim 5 nm. At larger thicknesses ($>$ 5 nm), absorption becomes significant which may lead to inaccurate measurements. For the X-ray reflection measurements, we used a PANalytical X'Pert PRO X-ray diffraction system to do reflectometry analysis and obtain the film thickness. The Pt film density was also characterized by XRR by averaging multiple points on a sample at each film thickness studied. Scanning electron microscopy (SEM) and atomic force microscopy (AFM) were used to determine the Pt film morphology. X-ray photoelectron spectroscopy (XPS) analysis was performed to investigate the film composition, and Auger electron spectroscopy (AES) (Evans Analytical Group) was used for elemental mapping of the patterned structure. Four-point probe measurement was used to determine the Pt film resistivity.

The growth rate was determined by dividing the film thickness measured by ellipsometry by the number of ALD cycles. In the investigation of growth rate dependence on ALD conditions, multiple locations on at least two samples obtained from separate 100 cycle ALD processes were probed to determine thickness. To probe the ODTS film degradation in the ALD Pt process, we used XPS to determine the resulting ODTS film thickness; after curve fitting of the XPS C 1s, O 1s, and Si 2s core level peaks, an electron escape depth calculation was carried out to estimate the film thickness.

Results and Discussion

Atomic layer deposition of platinum thin films.— Pt thin-film deposition by ALD was initially studied by Aaltonen et al.⁵ Using the same precursors, MeCpPtMe₃ and air, we deposited Pt thin films by ALD on both Si and YSZ substrates and explored the optimal ALD conditions that were characteristic of our system.³¹ Here, we highlight only a few significant points. First, we identified the optimal deposition temperature in our system to be 285°C. Based on the previously reported data,⁵ we investigated substrate temperatures between 225 and 345°C. We observed that from 225 to 285°C, the Pt film growth rate increases with temperature, stays constant at \sim 0.4 Å/cycle from 285 to 300°C, then increases again in the temperature range from 310 to 345°C. The growth rate behavior is in good accordance with that reported by Aaltonen et al.⁵ The larger growth rate at higher substrate temperatures suggests partial decomposition of the precursor and formation of nonvolatile cracking products; this decomposition must be avoided in the ALD process because it destroys the self-saturation growth mechanism and may lead to Pt films with higher impurity content. Furthermore, it may also result in the failure of the area selective ALD process. For the subsequent experiments, a deposition temperature of 285°C was used to allow a relatively high growth rate while minimizing the possibility of precursor decomposition.

We also probed the optimal precursor feed temperature. The Pt precursor (melting point 31°C) as purchased was an off-white powder. Measurements at room temperature (\sim 21°C) revealed no observable pressure increase when the precursor line was opened to the ALD reactor, and no growth was measured. Hence, in a divergence from the setup of Aaltonen et al.,⁵ we elevated the platinum precursor temperature in all of our ALD processes. The Pt precursor temperature range investigated here was from 32 to 75°C. The growth rate was observed to increase with temperature when the metal precursor temperature was $<$ 50°C and reached a constant value at temperatures $>$ 50°C. Thus, the optimal metal precursor temperature was set at 50°C, and this temperature was also used for further experiments.

We observed an interesting effect of the length of the air precursor pulse. In studies of the growth rate dependence on the air pulse time over the range of 1.5–3 s, the growth rate was observed to rise with air pulse time, reaching a peak value of 0.43 Å per cycle when the air pulse time is at 2 s, then decrease at longer air pulse times. The correlation of growth rate with the air pulse time is different from that observed by Aaltonen et al., who reported saturation at longer air pulse times.⁵ There are several possible explanations for the decreasing growth rate observed here. The growth rate may decrease if the adsorption process of MeCpPtMe₃ is reversible, with Pt precursor desorbing from the substrate with time. This explanation is supported by the fact that the film growth rate did not reach saturation, but continued to decrease from 0.5 Å/cycle to 0.29 Å/cycle, when the N₂ purging time after the Pt precursor dose was increased from 7 s to 60 s. Another possible reason is that impurities in the dry air source may deactivate active sites on the substrate.³²⁻³⁶

The composition of the Pt films deposited by ALD was investigated by X-ray photoelectron spectroscopy (XPS). XPS spectra of a Pt film deposited by 500 ALD cycles both as-deposited and after mild sputtering are shown in Fig. 1. The as-deposited film was found to consist of 46% platinum, 46% carbon, and 8% oxygen. The pres-

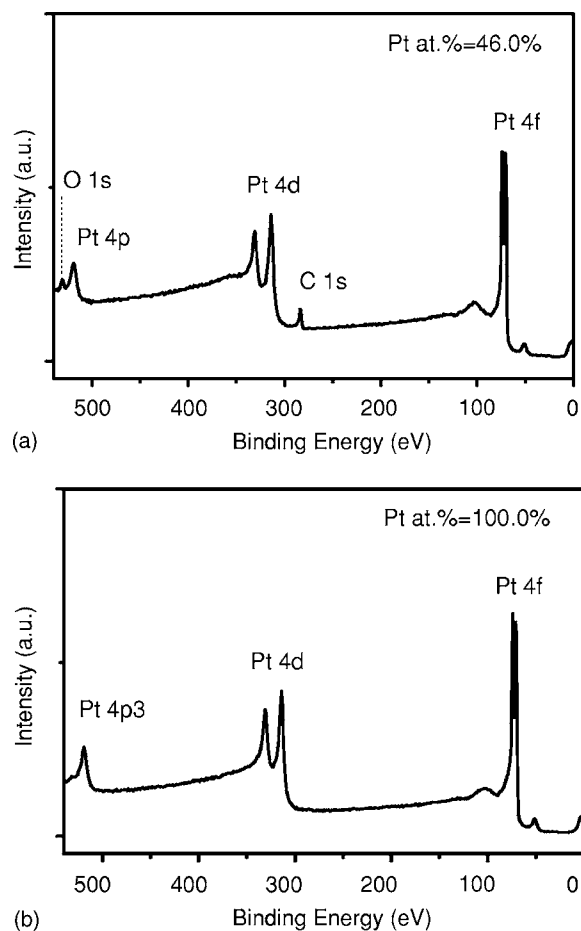


Figure 1. XPS spectrum of a 20 nm Pt film on a Si substrate (a) before argon ion sputtering and (b) after removing a ~ 1 nm superficial surface layer by argon ion sputtering. ALD conditions: substrate temperature: 285°C; precursor temperature: 50°C; dosing time: 2 s; purge time: 12 s; ALD cycles: 500 cycles.

ence of carbon and oxygen can arise from environmental contamination occurring after the ALD process. To confirm this, we used in situ argon ion sputter etching to remove the topmost layers. Fig. 1b, taken after sputtering ~ 1 nm of material from the surface, reveals that the film is pure Pt with no observable contaminants to 0.1%

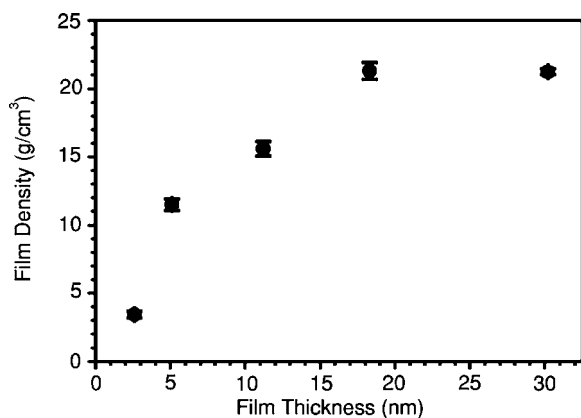


Figure 2. The film density of the as-deposited Pt film vs film thickness. ALD conditions: substrate temperature: 285°C; precursor temperature: 50°C; dosing time: 2 s and purge time: 12 s. The error bars reflect one standard deviation.

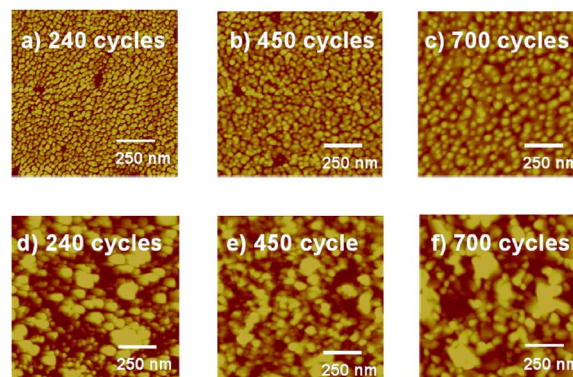


Figure 3. (Color online) AFM images of Pt thin films vs the number of ALD cycles. (a)–(c) are Pt films on native oxide coated Si wafers, (d)–(f) are Pt films on YSZ substrates. The rms roughness values of Pt films on Si substrates are 1.5–2.8 nm, and the rms roughness of Pt films on YSZ substrates are 2.2–3.2 nm. The Z range of the AFM images is 8 nm.

sensitivity. X-ray reflectometry was employed to investigate the as-deposited Pt film density as a function of film thickness. Figure 2 shows that the film density increases with the film thickness and is saturated at 21.3 g/cm³ for films thicker than 18.3 nm. Because the bulk density is 21.4 g/cm³, the results indicate that the Pt films thinner 18.3 nm are discontinuous and porous. This discontinuous structure may be formed due to the island growth mechanism, in which islands of fixed lateral dimension first grow to a given height and then spread to cover the surface.^{33,34}

Evolution of the surface morphology of the as-deposited Pt films was examined by AFM as the number of ALD cycles was increased. AFM images collected after 240, 450, and 700 ALD cycles are shown in Fig. 3 for both Si and YSZ substrates. The rms roughness of the Pt films on both substrates, determined by AFM, are listed in Table I, together with Pt film thickness measured by X-ray reflectometry. The AFM study indicates that the rms roughness decreases with increasing number of ALD cycles. RMS roughness for a 30 nm Pt film was as low as 2.2 nm on YSZ, indicating that the Pt films are quite smooth. The Pt films deposited on the Si substrates were slightly less rough than those deposited on the YSZ substrates, likely reflecting the smoother starting surface of Si compared to YSZ (0.3 nm vs 3.7 nm). In addition to morphology, the resistivity of the films was also measured with the four-point probe method, and the results are included in Table II, which shows that the resistivity decreases with increasing film thickness, with a resistivity of 18.3 $\mu\Omega$ cm measured for the 30 nm thick film. This resistivity compares reasonably well to the bulk Pt value (10.8 $\mu\Omega$ cm).³⁷

To investigate the temperature dependence of the film morphology and resistivity, a postannealing process was carried out in an O₂ environment for 30 min at each temperature. Table I lists the rms

Table I. RMS roughness of as-deposited and postannealed Pt films measured by AFM. The film thickness was determined by XRR. Note: rms roughness of YSZ substrate and Si substrate was 3.7 nm and 0.3 nm, respectively, prior to deposition.

Pt film thickness (nm)	RMS of Pt films on YSZ substrate (nm)			RMS of Pt films on Si substrate (nm)		
	As-deposited	350°C	550°C	As-deposited	350°C	550°C
11.2	3.2	3.5	3.5	2.8	2.1	1.6
18.3	2.5	2.9	3.5	1.8	1.6	1.9
30.2	2.2	2.6	2.6	1.5	1.5	4.8

Table II. Resistivity ($\mu\Omega$ cm) of as-deposited and postannealed Pt films. Dash (–) indicates no measurement was made.

Pt film thickness (nm)	Resistivity of Pt films on YSZ substrate ($\mu\Omega$ cm)			Resistivity of Pt films on Si substrate ($\mu\Omega$ cm)
	As-deposited	350°C	550°C	As-deposited
11.2	31.3	23.3	22.5	–
18.3	22.6	18.8	–	41.9
30.2	18.3	17.2	15.8	16.3

roughness of both the as-deposited and the postannealed films at two different annealing temperatures (350 and 550°C). Measurements were made on two separate samples for each entry in Table I. The data show that the rms roughness of the postannealed films deposited on YSZ is slightly increased compared to that of the as-deposited films. An exception is that of the 30.2 nm Pt film on Si, for which there is a large increase in the rms roughness on annealing to 550°C; this increase in the film rms is likely due to agglomeration of Pt islands at elevated temperatures. Table II lists the resistivity of both as-deposited and postannealed Pt films deposited by ALD. Post-ALD annealing studies show that the resistivity of the Pt film remains low for temperatures up to at least 550°C, which suggests that Pt is an excellent catalyst and electrode material for SOFCs operated at low temperature (<600°C).

Area-selective ALD of platinum.— In order to carry out area-selective ALD of Pt, a good resist system is needed to block the substrate surface active sites. In our studies, ODTS SAMs were explored as the ALD resist. In the formation of the ODTS SAM, the chlorine atoms in the ODTS molecules are hydrolyzed by reacting with trace water. The hydrolysis step is followed by the reaction between the molecular hydroxide groups and the silanol groups present on the surface to form a covalent Si–O–Si bond, resulting in a monolayer containing molecules that are both covalently linked to the substrate as well as to their neighbors. Some reaction between precursors is thought to occur in solution, leading to small molecular clusters that then react to form Si–O–Si bonds at the surface.^{19,27–29} However, too much water present in the solution will result in bulk polymerization of the silane before it reacts with the surface. Under this condition, ODTS films will grow as islands, which have a high density of defects, instead of as a smooth, densely packed monolayer.^{19,38,39} Thus, care was taken to control the amount of water in the glove box used for the SAM experiments. All Si–Cl bonds were fully reacted in the hydrolysis process, as indicated by the absence of chlorine in an XPS analysis of the ODTS-coated substrates.

Following the ODTS SAM formation, samples were characterized by ellipsometry and water contact angle. A systematic study of the deactivating effect of octadecyltrichlorosilane (ODTS) SAMs toward Pt ALD was carried out. The results are shown in Fig. 4, which also includes information on the silylation time dependence for ODTS SAM formation by the measurement of film thickness and contact angle of the SAM. The film thickness of the ODTS SAM increased with SAM-formation time until a plateau was reached at values of 26 Å, and the contact angle was found to exhibit similar behavior, reaching a maximum value of 110°, which is consistent with previous studies.^{10,19,39,40} The contact angle measurement reveals the hydrophobicity of the monolayer, and the change in the contact angle roughly indicates the extent of the monolayer surface coverage as well as the variation in the surface chemical composition of the substrate.^{41–44} Approximately, 2 h were required for the water contact angle of the ODTS SAM to reach a plateau, indicating that the formation of a closely packed monolayer takes at least 2 h.

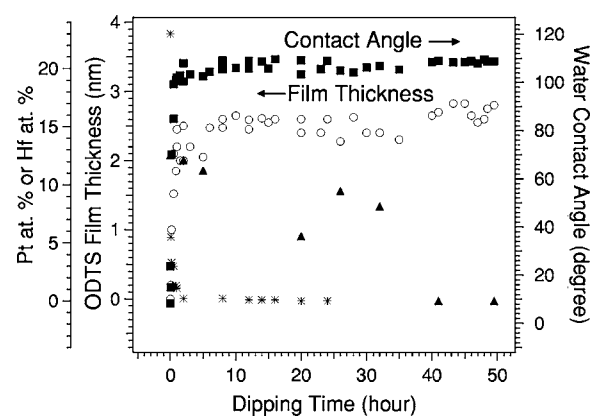


Figure 4. Time dependence of ODTS film formation and its ALD blocking effectiveness on 100 cycles of Pt ALD. Water contact angle measured on the ODTS film (■), ODTS film thickness (○), Hf atomic percent (▲) and Pt atomic percent (*). Data for HfO₂ taken from Ref. 18.

Another set of ODTS-coated substrates prepared in the same process was introduced into the ALD reactor for 100 cycles of atomic layer deposition of Pt. XPS studies of these substrates after the Pt ALD process show that the Pt atomic percent (Fig. 4) is inversely correlated with the contact angle and thickness of the monolayer resist. The Pt atomic percent dropped very quickly to below the XPS sensitivity limit when the dipping time was above 12 h. This selectivity was likely achieved because there were no active sites presented on the ODTS-covered surface, preventing the nucleation of Pt precursors and subsequent film growth.^{5,8}

In an earlier set of studies, we investigated the ability of ODTS to block HfO₂ ALD.^{10,11} To compare the ODTS blocking effect on HfO₂ vs Pt ALD, the corresponding Hf atomic percent data as a function of SAM formation time is also included in Fig. 4. Although the trend is similar, it takes 42 h to fully block the HfO₂ ALD process while only 12 h are needed to fully block the Pt ALD growth. Thus, the Pt ALD growth is more easily deactivated by the SAM, as indicated by the absence of observable Pt on ODTS films with shorter silylation times. Here, we speculate as to two possible reasons for the difference between Pt and HfO₂. The first explanation is based on the difference of the sizes of the two metal precursors. For the growth of HfO₂ and Pt, hafnium tetrachloride and (methylcyclopentadienyl)trimethylplatinum were used as the metal precursors, respectively. The ligands of MeCpPtMe₃ are larger compared to that of the hafnium tetrachloride. For loosely packed ODTS film, there are defects, or pinholes, present in the surface.¹¹ If the size of the pinholes is larger than that of the hafnium precursors, then the precursor can diffuse through the pinholes and react at the substrate to nucleate HfO₂ growth. If the pinhole size is smaller than that of the MeCpPtMe₃ molecule, then the Pt precursor will not reach the surface active sites due to steric hindrance. Thus, Pt ALD growth can be deactivated even by an imperfectly packed ODTS SAM. Besides the geometric point of view, the inherent chemical reactivity of the precursors used in the two processes may account for the difference. The ability to block ALD with shorter silylation times for the Pt process suggests that the Pt precursor and dry air may not be as reactive as hafnium tetrachloride and water toward the underlying oxide-coated Si substrate. In addition, the difference of oxygen affinity between the Hf and Pt may play a role here. In a study by Park et al.,¹⁷ Ru nucleation was also found to be less sensitive to the quality of the monolayer surface than deposition of Hf or Zr oxide¹¹ and Ti based films.⁴⁵ This effect was attributed to the lower oxygen affinity of Ru, making the Ru precursor less likely to penetrate the monolayer and react with oxide present at the Si/monolayer interface. All these arguments noted above support the conclusion that the conditions for blocking the Pt ALD are less stringent compared to those needed to block HfO₂ growth.

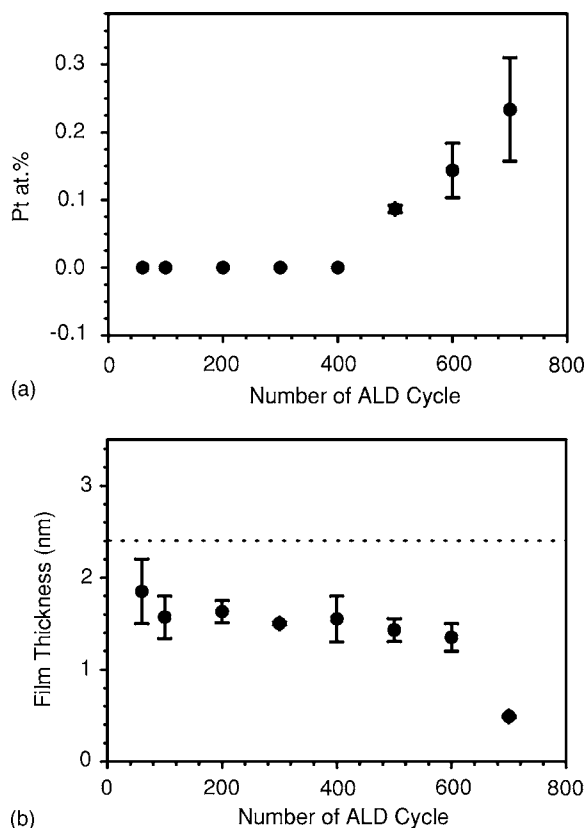


Figure 5. (a) Deactivating effectiveness of a densely packed ODTS film against Pt ALD as measured by Pt atomic percent and (b) film degradation during the ALD process indicated by the change of its film thickness. Dotted line indicates the thickness of a densely packed ODTS monolayer. Error bars show one standard deviation.

To investigate how well the ODTS SAMs block Pt ALD for higher numbers of ALD cycles, studies were carried out up to 700 cycles. In these studies, densely packed SAMs were formed by immersion into ODTS solution for 48 h.²³ Then, the ODTS-coated substrates were introduced into the reactor for varying numbers of ALD cycles. An XPS study was performed to examine the resulting Pt atomic percent and estimate the degradation in the SAM film thickness. The results are shown in Fig. 5. Figure 5a shows that below 400 cycles, there is no observable Pt within the detection limit of the XPS spectrometer. This result indicates that the Pt ALD reaction is completely deactivated by ODTS when the number of ALD cycles is <400 under the given ALD conditions. Figure 5b shows the ODTS film thickness estimated with XPS after the given number of ALD cycles. Each measurement was repeated twice. The thickness of the initial ODTS film, with no exposure to the ALD reactor, is shown as a dashed line. It is clear that the ODTS film thickness decreased relative to the control even for the lowest number of ALD cycles studied. Furthermore, the degradation seems to get worse with increasing number of ALD cycles. ODTS monolayers are reported to start degrading at 200°C, and the stability decreases with increasing temperature.^{25,46,47} Thus, the observed loss of ODTS film thickness is likely due to the thermal decomposition of the SAM at the elevated temperature of 285°C. However, the degraded ODTS film still retained the ability to block ALD at the surface, as is evident by the XPS measurements shown in Fig. 5a.

In addition to Si, area-selective ALD experiments were also carried out on YSZ. Figure 6 shows XPS survey scans of the samples after 50 cycles of Pt ALD. For the native oxide-coated Si (Fig. 6a) and YSZ (Fig. 6c) substrates, there are apparent Pt peaks and the Pt atomic percent are 29.3 and 33.0%, respectively, while there is no

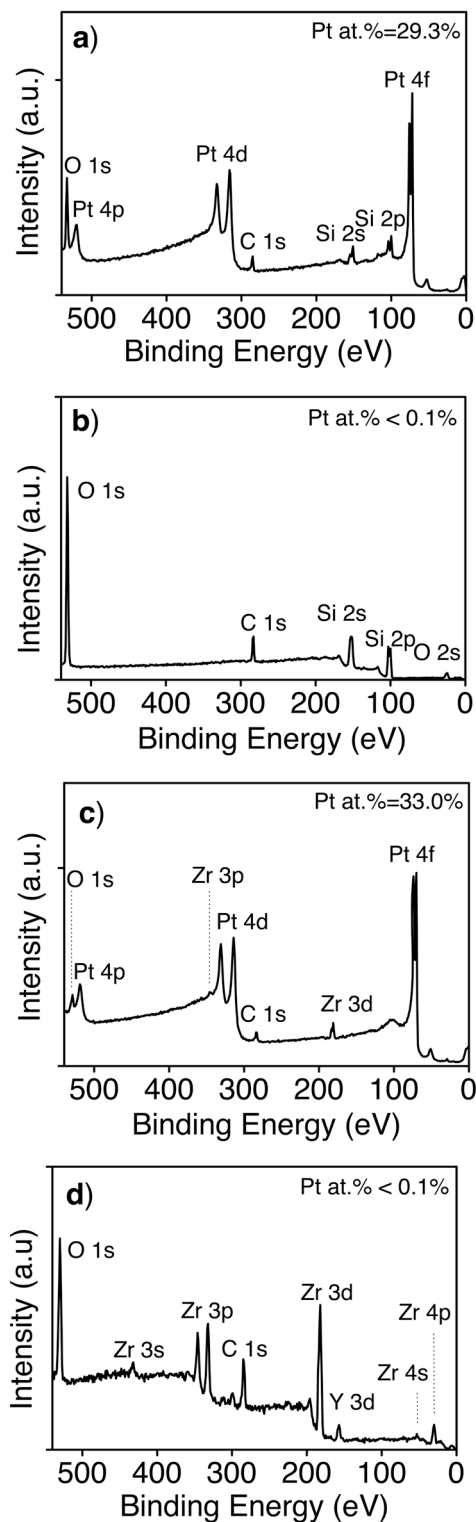


Figure 6. Deactivating effectiveness of the fully dense ODTS SAMs. (a) and (c) are XPS spectra of samples following Pt ALD on ODTS-free Si and YSZ substrates, respectively; (b) and (d) are spectra of samples following Pt ALD on ODTS-coated Si and YSZ substrates, respectively. ALD conditions: substrate temperature: 285°C; precursor temperature: 50°C; dosing time: 2 s; purge time: 60 s; ALD cycles: 50 cycles.

evidence of Pt on the ODTS-coated Si (Fig. 6b) and YSZ (Fig. 6d) substrates. Thus, excellent deactivation can be obtained by using the ODTS SAM as a resist on both Si and YSZ. For ALD to occur, the

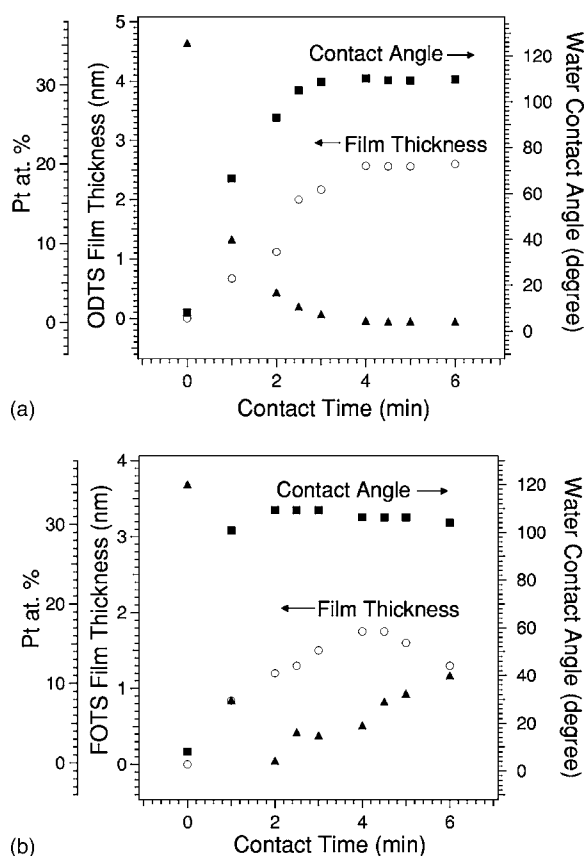


Figure 7. Deactivating effect of μ CP-prepared (a) ODTS and (b) FOTS films on Pt ALD on Si substrates. Water contact angles (■) and thickness (○) measured on the ODTS and FOTS films; Pt atomic percent (▲) on ODTS- and FOTS-coated Si.

solid substrate must contain reactive sites and the reactants must be sufficiently reactive with those sites at the reaction temperature. According to the proposed Pt ALD growth mechanism by Aaltonen et al.,⁹ Pt precursors need to nucleate onto the oxygen present on the substrate to facilitate the film growth. On both native oxide-coated Si and YSZ substrates, Pt deposition occurs due to the presence of oxygen on the substrate. In contrast, the ODTS-coated substrates are terminated with methyl group and do not have any active functional group to react with the Pt precursor. Thus, as expected, there was no Pt growth on the ODTS-coated substrates.^{5,9,11,15,48}

Once the facility of ODTS as a resist was confirmed, patterned octadecylsiloxane SAMs were made on the Si and YSZ substrates using μ CP. In this process, the contact time was found to be crucial to the integrity of the pattern transfer. When the stamp was removed too quickly, loss of pattern resolution occurred because the ODTS was still wet and spread. However, long contact times between the PDMS and the substrate sometimes resulted in the breakage of the PDMS stamp such that parts of the stamp remained on the substrate, or alternatively the “ink” remained on the stamp. Thus, before investigating the area selective ALD process, we first explored the optimal contact time by transferring a nonpatterned film onto the substrate using a blank PDMS stamp. For this study, we examined both 10 mM ODTS and 10 mM FOTS solutions to form the ALD resists. Figure 7 shows the time dependence of ODTS and FOTS film formation using water contact angle and ellipsometry analysis and the resulting Pt atomic percent after ALD on the corresponding SAMs. Similar to the results for the SAMs formed through solution phase reaction (Fig. 4), the measured contact angles in μ CP increase with contact time until they reach a plateau for both ODTS and FOTS. The contact angle of the FOTS film reaches a saturation

value of 109° after 2 min, while the ODTS film takes 4 min to reach 110° . These two limiting contact angle values are consistent with the literature.¹¹

Although the contact angle trends are similar between ODTS and FOTS, differences can be seen in the film thickness measurements. The ODTS film thickness, shown in Fig. 7a, increased with contact time then leveled off by 4 min at a thickness of 25.6 Å. The FOTS film thickness, shown in Fig. 7b, peaked at 17.5 Å with a contact time 4–4.5 min, then decreased for longer contact times. We note that the saturated ODTS film thickness and the peak thickness value of the FOTS films are in good agreement with the literature.¹¹ Although we do not fully understand the decrease in the thickness of FOTS SAMs with increased stamping time, the results suggest that the FOTS film may become partially bound to the PDMS stamp at longer times, so that when the stamp is removed, it leaves behind at the substrate an incomplete film with high defect density. The differences may stem from the higher reactivity of FOTS than ODTS due to presence of the fluorocarbon tail, since the CF_3 substitution on the γ -C exerts a large inductive effect on the silicon atom of the incoming head group, making it a better electrophile for nucleophilic attack by the oxygen atom of SiOH groups.⁴⁹ We speculate that the measured water contact angles of these incomplete FOTS films remain high due to the highly hydrophobic fluorocarbon tail, as well as from increased film roughness.^{11,19,41}

The Pt concentrations measured after ALD on the films follow the film thickness behavior. The XPS studies of these substrates after the Pt ALD process show the Pt atomic percent on the FOTS coated substrates drops more quickly than it does on the ODTS-coated substrates, and reaches a minimum at 2 min. This trend suggests that if densely packed FOTS films could be achieved, they may have the potential to deactivate Pt ALD growth in a shorter time compared to ODTS films. However, among the microcontact printed SAMs, ODTS serves as a better ALD resist, shown by its higher deactivation ability. The minimum Pt composition achieved on the FOTS and ODTS coated substrates are 0.3% and $<0.1\%$, respectively. The increase of the Pt atomic percent after the minimum at 2 min on the FOTS-coated substrates may be due to a high density of defects in the films formed with too long a stamping time.

It is interesting to compare the two SAM fabrication approaches: microcontact printing and solution phase deposition. First, films fabricated in either method have similar saturation film thickness and contact angles. For ODTS SAMs, the maximum film thickness and contact angle are ~ 26 Å and $\sim 110^\circ$, respectively, both by microcontact printing and by solution deposition. This suggests that the ODTS molecules may be of similar order and tilt angles in the final phase of the films fabricated in both methods.³⁹ Second, to achieve SAMs of the same quality, the characteristic time is significantly shorter when microcontact printing is used. We can use the blocking effect on ALD as a sensitive probe of SAM quality. To fully deactivate the Pt ALD growth, ODTS SAMs developed in the solution phase need 12 h formation time, whereas the microcontact printed SAMs need under 4 min, as shown in Fig. 4 and 7a, respectively. The shorter formation time of the microcontact printed ODTS film may be attributable to the following effects. Both methods started with an ODTS solution of the same concentration (10 mM). However, the “ink” on the PDMS stamp is dried by nitrogen flow to evaporate the toluene solvent, resulting in an ODTS solution with significantly higher concentration. This elevated concentration will facilitate both stages of the formation of the ODTS SAM, including the surface-head group reaction and the surface crystallization process.^{19,39} Thus, fabrication of SAMs through μ CP is recommended as a more efficient way of depositing the ALD resist.

Patterning.— The PDMS stamps used in the procedure of area selective ALD consisted of a grid pattern with feature sizes ranging from 2 μm to 50 μm . Inked with an ODTS solution, the PDMS stamps were placed in contact with the Si and YSZ substrates for 5 min. The result is a negative, hydrophobic pattern of the original master transferred onto the substrates. Figure 8a shows an SEM

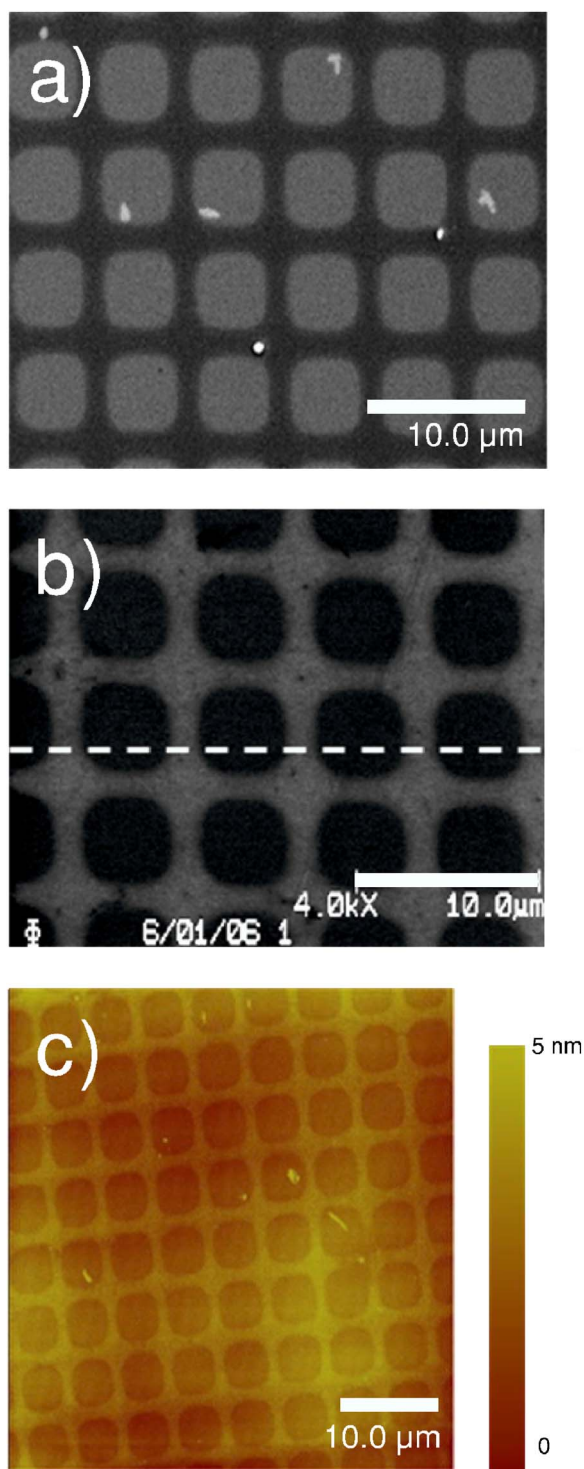


Figure 8. (Color online) Microscopy images of stamped substrates designed for a $2\ \mu\text{m}$ wide grid line with $4\ \mu\text{m}$ spacing. (a) and (b) are SEM images of patterned ODTs on YSZ before and after area-selective ALD, respectively; (c) is the AFM image of the ODTs-patterned YSZ substrate after Pt ALD. In (a), the brighter squares are where ODTs was stamped. For the AFM image, the Z range is 5 nm and the Pt film within the grid regions is $\sim 3.5\ \text{nm}$ thick.

image of the patterned SAMs on YSZ produced from a stamp with a mesh structure containing $4\ \mu\text{m}$ squares separated by $2\ \mu\text{m}$ spaces. The bright square regions are those of ODTs-coated YSZ areas, whereas the dark regions are the ODTs-free YSZ areas. The patterned monolayers retain the dimensions of the masters without noticeable chemical spreading.

After μCP using a $4\ \mu\text{m} \times 2\ \mu\text{m}$ patterned stamp (generating $4\ \mu\text{m}$ squares of ODTs SAMs separated by $2\ \mu\text{m}$ lines), Pt thin films were selectively deposited onto the patterned Si and YSZ substrates by ALD using MeCpPtMe_3 and air as ALD precursors. The selective ALD of the Pt thin films was carried out at a substrate temperature of 285°C , and the number of ALD cycles in all the processes was kept at 100.

Figures 8b and c show an SEM image and an AFM image, respectively, of the micropatterned YSZ substrates after area selective ALD of Pt thin films. The contrast inverts in the SEM image of Fig. 8b relative to that of Fig. 8a, and the raised part of the Pt grid structure can be seen in the AFM image of Fig. 8c, indicating that Pt deposition occurs in the regions that are not stamped with ODTs. The rounding of the edges observed in the pattern arises from the photolithography step during the fabrication of the silicon master at these small size scales. In addition to SEM and AFM, Auger electron spectroscopy (AES) was used to look at the micropatterned Pt grid structures on YSZ. The AES instrument used in these studies has a spatial resolution of $\sim 10\ \text{nm}$ and a sensitivity of 0.1% for Pt. Figures 9 and 10 illustrate the AES analysis of the patterned mesh structures at high spatial resolution. Auger survey spectra, which provide information on the relative concentrations of elements, were collected in both the ODTs-coated and the uncoated regions of the YSZ substrate. The survey spectra, shown in Fig. 9, reveal that in the ODTs-coated YSZ regions (Fig. 9a), the Pt signal is below the AES detection limit (0.1%), whereas in the ODTs-free YSZ regions (Fig. 9b), the Pt atomic percent is 24%, a value that is comparable to that for nonchemically treated YSZ reference samples in the same ALD run. This result indicates that the Pt thin films are selectively deposited only onto the ODTs-free regions of the substrate and are blocked at the regions coated by ODTs.

Auger line scans were used to measure the peak intensity of the Pt and C and Zr Auger peaks as a function of position along the defined line displayed in Fig. 8b. In Fig. 9c, the Pt, C, and Zr Auger peaks show the expected intensity alternation. The edges of the lines are not extremely sharp, likely because the edge of ODTs films contains a higher density of defects in contrast with interior of the film.⁵⁰⁻⁵² This high density of defects will enable Pt precursors to nucleate at the substrate and thus allow atomic layer deposition of Pt. Note that the edge effect laterally occupies $< 0.5\ \mu\text{m}$, suggesting that area-selective ALD of Pt can be achieved at submicrometer spatial resolution using this combined ALD- μCP technique.

AES elemental mapping of Pt, C, and Zr were also conducted based on the test pattern. Scanning Auger maps (Fig. 10) were acquired by measuring the peak intensity of the selected elements as a function of beam position. The scanned area is defined in the SEM image in Fig. 8b. The maps show the relative elemental distributions (peak intensity) as a pixel intensity; that is, the greater the Auger peak intensity, the brighter the pixel value. Figures 10a-c display the elemental mapping of Pt, C, and Zr, respectively. In Fig. 10a, the bright regions indicate the presence of Pt while the dark areas indicate the absence of Pt. Pt clearly is deposited in the desired grid pattern. Figure 10b showed that more C is present in the square areas due to the coated ODTs monolayer, whereas Fig. 10c shows that less Zr (proportionately) is in the ODTs-free areas due to the presence of Pt at the surface. Both the SEM image (Fig. 8b) and the AES image (Fig. 10) have the same shape, which indicates successful confinement of Pt deposition to the ODTs-free region only. All the results from SEM, AFM, and AES confirm that the Pt patterns were well defined and directed with high selectivity by the patterned SAMs generated with microcontact printing.

The method presented here could, in principle, provide high selectivity, high spatial resolution, and compatibility with more complex starting substrates than the flat substrates tested in this work. We plan to integrate these Pt thin films as electrode, catalyst, and current collect grid into SOFC's in studies to improve fuel cell performance at lower operating temperature.

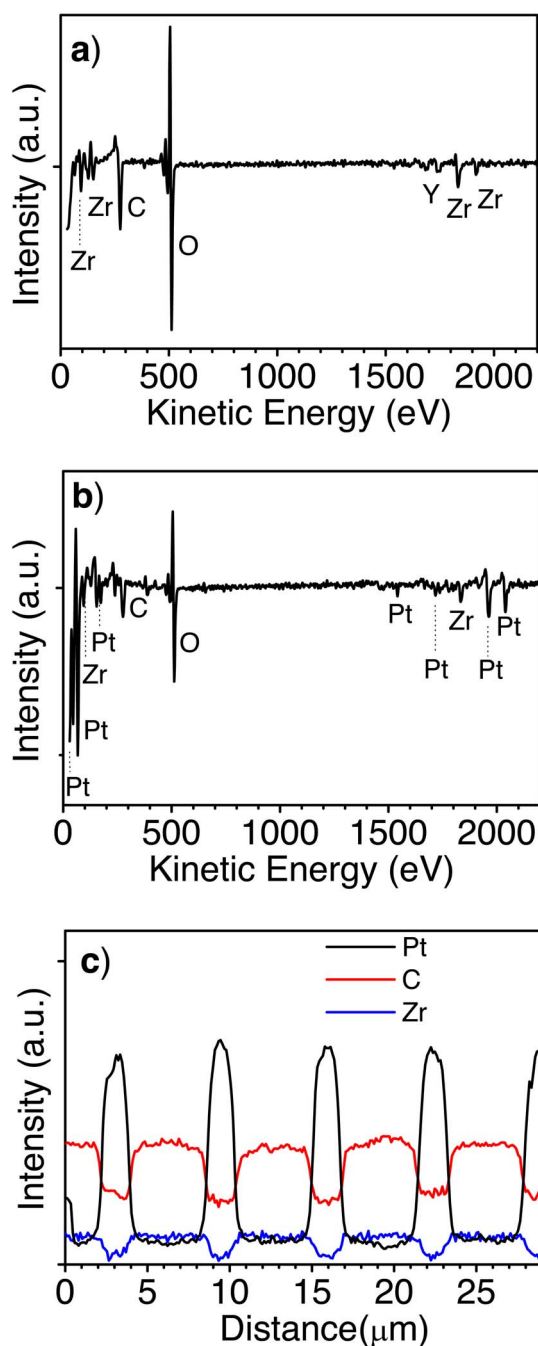


Figure 9. (Color online) Auger survey spectra of the areas of (a) an ODTs-coated region and (b) an ODTs-free region of YSZ, for a $4\ \mu\text{m} \times 2\ \mu\text{m}$ patterned substrate. (c) Defined AES line scan showing alternation of Pt, C, and Zr signals.

Conclusion

In this work, Pt films were deposited using ALD on YSZ substrates for application in solid oxide fuel cells. Films of high purity and low resistivity were obtained, and studies show that after annealing the films in oxygen, the films retain similar resistivities and rms roughness from the deposition temperature up to at least 550°C . High-quality ODTs SAMs were fabricated through both solution phase and μCP , and the latter approach was illustrated to be much more efficient in forming a SAM of good quality with shorter silylation times. ODTs SAMs were employed as an ALD resist and Pt ALD growth was shown to be more easily deactivated by ODTs

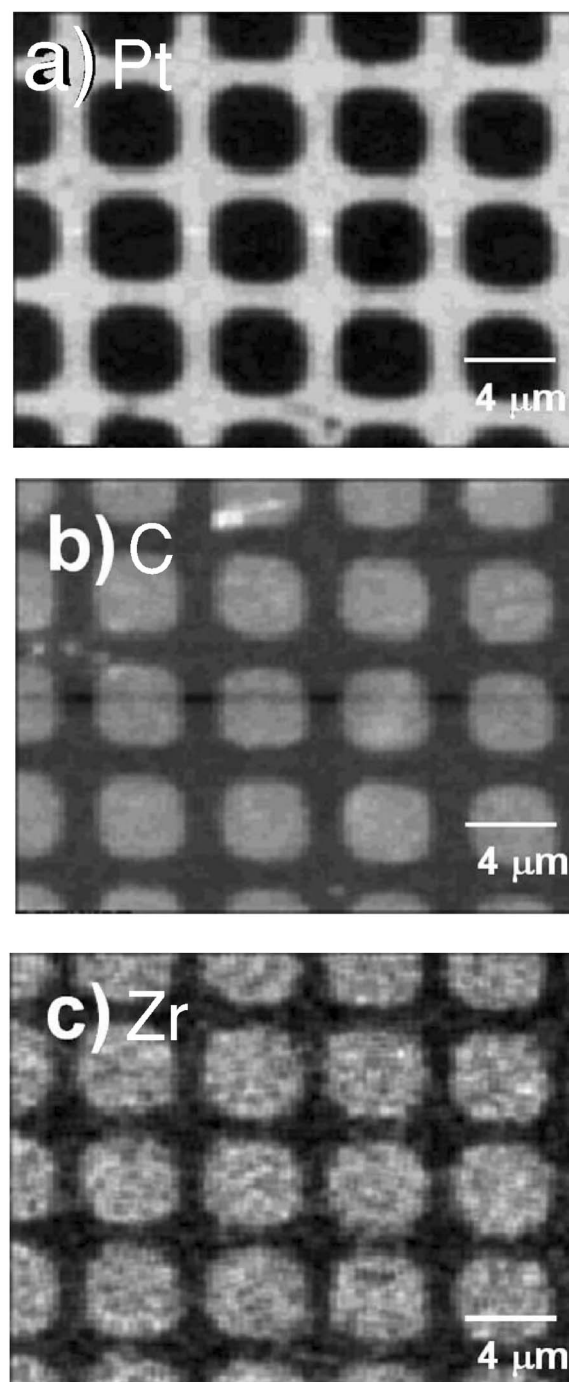


Figure 10. Auger elemental maps for (a) platinum, (b) carbon, and (c) zirconium on the micropatterned grid structure after area selective ALD of Pt on YSZ.

SAMs compared to the HfO_2 ALD process. Furthermore, patterned Pt thin films with high spatial resolution have been achieved using atomic layer deposition on microcontact printed Si and YSZ substrates. ODTs SAMs were used here as an ALD resist to direct the area selective deposition of the Pt thin film. The Pt thin-film selectively grows only on the ODTs-free region because the octadecylsiloxane monolayers act to block reactive functional groups at the substrate. We plan to integrate this Pt grid structure into SOFC fuel cells for use as the current collect grid, electrode, and catalyst.

Acknowledgments

The authors thank Sandeep Giri and Dr. Jeffrey S. King for their help with the ALD of Pt.

References

- J. Sinfelt, *Catalysts Discoveries, Concepts, and Applications*, Wiley, New York (1983).
- S. M. Sze, Editor, *VLSI Technology*, 2nd ed. McGraw-Hill, New York (1988).
- R. E. Jones and S. B. Desu, *MRS Bull.*, **21**, 55 (1996).
- U.S. Department of Energy, *Fuel Cell Handbook*, 7th ed., Morgantown, West Virginia (2004).
- T. Aaltonen, M. Ritala, T. Sajavaara, J. Keinonen, and M. Leskelä, *Chem. Mater.*, **15**, 1924 (2003).
- M. Ritala and M. Leskelä, *Handbook of Thin Film Materials*, Academic Press, New York (2002).
- T. Suntola, *Handbook of Thin Film Process Technology*, B1.5:1, Institute of Physics, Bristol, U.K. (1995).
- T. Aaltonen, M. Ritala, Y. L. Tung, Y. Chi, K. Arstila, K. Meinander, and M. Leskela, *J. Mater. Res.*, **19**, 3353 (2004).
- T. Aaltonen, A. Rahtu, M. Ritala, and M. Leskela, *Electrochem. Solid-State Lett.*, **6**, C130 (2003).
- R. Chen, H. Kim, P. C. McIntyre, and S. F. Bent, *Appl. Phys. Lett.*, **84**, 4017 (2004).
- R. Chen, H. Kim, P. C. McIntyre, and S. F. Bent, *Chem. Mater.*, **17**, 536 (2005).
- R. Chen, D. W. Porter, H. Kim, P. C. McIntyre, and S. F. Bent, *Mater. Res. Soc. Symp. Proc.*, **917**, E11–05 (2006).
- J. P. Lee, Y. J. Jang, and M. M. Sung, *Adv. Funct. Mater.*, **13**(11), 873 (2003).
- M. M. Sung, in *EUROCVI-15. 15th European Conference on Chemical Vapor Deposition*, A. Devi, R. A. Fischer, H. Parala, M. D. Allendorf, and M. L. Hitchman, Editors, PV 2005-09, p. 203, The Electrochemical Society Proceedings Series, Pennington, NJ (2005).
- E. K. Seo, J. W. Lee, H. Sung-Suh, and M. M. Sung, *Chem. Mater.*, **16**, 1878 (2004).
- M. H. Park, Y. J. Jang, H. M. Sung-Suh, and M. M. Sung, *Langmuir*, **20**, 2257 (2004).
- K. J. Park, J. M. Doub, T. Gougousi, and G. N. Parsons, *Appl. Phys. Lett.*, **86**, 051903 (2005).
- M. Yan, Y. Koide, J. R. Babcock, P. R. Markworth, J. A. Belot, T. J. Marks, and R. P. H. Chang, *Appl. Phys. Lett.*, **79**, 1709 (2001).
- A. Ulman, *Chem. Rev. (Washington, D.C.)*, **96**, 1533 (1996).
- J. D. Swalen, D. L. Allara, J. D. Andrade, E. A. Chandross, S. Caroff, J. Israelachvili, T. J. McCarthy, R. Murray, R. F. Pease, J. F. Rabolt, K. J. Wynne, and H. Yu, *Langmuir*, **3**, 932 (1987).
- G. K. Jennings and P. E. Laibinis, *Colloids Surf., A*, **116**, 105 (1996).
- J. Shim, C. Chao, H. Hong, and F. B. Prinz, *Chem. Mater.*, **19**, 3850 (2007).
- M. De Ridder, R. G. Van Welzenis, and H. H. Brongersma, *Surf. Interface Anal.*, **33**, 309 (2002).
- U. Scrivivasan, M. R. Houston, R. T. Howe, and R. Maboudian, *J. Microelectromech. Syst.*, **7**, 252 (1998).
- G. J. Kluth, M. M. Sung, and R. Maboudian, *Langmuir*, **13**, 3775 (1997).
- B. C. Bunker, R. W. Carpick, R. A. Assink, M. L. Thomas, M. G. Hankins, J. A. Voigt, G. Sipola, M. P. de Boer, and G. L. Gulley, *Langmuir*, **16**, 7742 (2000).
- M. J. Geerken, T. S. van Zanten, R. G. H. Lammertink, Z. Borneman, W. Nijdam, C. J. M. van Rijn, and M. Wessling, *Adv. Eng. Mater.*, **6**, 749 (2004).
- R. R. Rye, G. C. Nelson, and M. T. Dugger, *Langmuir*, **13**, 2965 (1997).
- R. D. Peters, P. F. Nealey, J. N. Crain, and F. J. Himpsel, *Langmuir*, **18**, 1250 (2002).
- Y. Xia and G. M. Whitesides, *Angew. Chem., Int. Ed.*, **37**, 550 (1998).
- X. Jiang and S. F. Bent, *ECS Trans.*, **3**(15), 249 (2007).
- T. Suntola, *Mater. Sci. Rep.*, **4**, 261 (1989).
- R. L. Puurunen, *J. Appl. Phys.*, **97**, 121301 (2005).
- R. L. Puurunen, *Chem. Vap. Deposition*, **9**, 327 (2003).
- R. L. Puurunen, S. M. K. Airaksinen, and A. O. I. Krause, *J. Catal.*, **213**, 281 (2003).
- M. Putkonen, T. Sajavaara, L. S. Johansson, and L. Niinisto, *Chem. Vap. Deposition*, **7**, 44 (2001).
- Handbook of Chemistry and Physics*, 87th ed., D. R. Lide, Editor, Taylor and Francis, Boca Raton, FL (2007).
- F. Schreiber, *Prog. Surf. Sci.*, **65**, 151 (2000).
- D. K. Schwartz, *Annu. Rev. Phys. Chem.*, **52**, 107 (2001).
- S. R. Wasserman, Y. Tao, and G. M. Whitesides, *Langmuir*, **5**, 1074 (1989).
- S. H. Chen and C. W. Frank, *Langmuir*, **5**, 45 (1989).
- G. J. Sagiv, *J. Colloid Interface Sci.*, **112**, 457 (1986).
- D. L. Allara and R. G. Nuzzo, *Langmuir*, **1**, 45 (1985).
- W. A. Zisman, *Adhesion and Cohesion*, Elsevier, New York (1962).
- A. S. Killampalli, P. F. Ma, and J. R. Engstrom, *J. Am. Chem. Soc.*, **127**, 6300 (2005).
- M. M. Sung, G. J. Kluth, and R. Maboudian, *J. Vac. Sci. Technol. A*, **17**, 540 (1999).
- W. R. Ashurst, C. Carraro, R. Maboudian, and W. Frey, *Sens. Actuators, A*, **104**, 213 (2003).
- R. Puurunen, *Chem. Vap. Deposition*, **9**, 249 (2003).
- C. P. Tripp, R. P. N. Veregin, and M. L. Hair, *Langmuir*, **9**, 3518 (1993).
- R. B. A. Sharpe, B. J. F. Titulaer, E. Peeters, D. Burdinski, J. Huskens, H. J. W. Zandvliet, D. N. Reinhoudt, and B. Poelsema, *Nano Lett.*, **6**, 1235 (2006).
- A. J. Black, K. E. Paul, J. Aizenberg, and G. M. Whitesides, *J. Am. Chem. Soc.*, **121**, 8356 (1999).
- J. Aizenberg, A. J. Black, and G. M. Whitesides, *Nature (London)*, **394**, 868 (1998).